Applied Physics A (2023) 129:744
https://doi.org/10.1007/s00339-023-07015-z

Applied Physics A
Materials Science & Processing

Energy transfer characteristics of Nd^{3+}/Yb^{3+}-codoped phospho-silicate oxyfluoride glasses for ~ 1.0 µm laser applications

John Reddy Vootukuru[1] · Umamaheswari Hemakumar[2] · Padma Suvarna Renigunta[1] · Ravi Nirlakalla[3]

Received: 28 April 2023 / Accepted: 11 September 2023 / Published online: 4 October 2023

Abstract
Nd^{3+}/Yb^{3+}-codoped phospho-silicate oxyfluoride ($PNSBYNd_{0.5}Yb_{0.5}$) glasses were prepared by melt-quenching technique and the structural and photoluminescence (PL) properties were investigated. Scanning electron microscopy (SEM) and energy-dispersive X-ray spectroscopy (EDS) were used to assess glass microstructure and dispersed elements in the glass, respectively. A high-intense and broad Raman band appeared at 1179 cm^{-1} is attributed to υ_{as} (Si–O–Si) stretching vibrations of Q^3 units owing to high-alkali (Na^+) silicates and O–P–O $(PO)^{2-}$ symmetric stretching vibrations in Q^2 units. The g value of unpaired electrons in $PNSBYNd_{0.5}Yb_{0.5}$ glasses was assessed by electron spin resonance (ESR) spectra and found to be 2.0168, more significant than the standard value (2.0023). Various bismuth ionic states (Bi^{2+}, Bi^{3+} and Bi^{5+}) were related in the Bi $4f_{7/2}$ and Bi $4f_{5/2}$ XPS spectra; however, Bi^{3+} ions were dominated. From the PL spectrum, 874 nm band for the $^4F_{3/2} \rightarrow {}^4I_{9/2}$ transition of Nd^{3+} ions was dominated over 1053 nm emission band perceived in $PNSBYNd_{0.5}Yb_{0.5}$ glasses due to its quasi-three-level system. Energy transfer (ET) and cross-relaxations (CR) were unveiled in Nd/Yb-doped $PNSBYNd_{0.5}Yb_{0.5}$ glasses upon 808 nm diode laser excitation. The Nd^{3+} emission bands 874 and 1053 nm were merged with the Yb^{3+} band at 975 nm due to CR and ET from $^4F_{3/2} \rightarrow {}^2F_{7/2}$. The high intensity of the 975 nm laser may be a suitable candidate for NIR laser and amplification applications.

Keywords Neodymium/ytterbium · ESR · Optical · PL emission · Energy transfer

1 Introduction

Rare earth (RE) ions-doped materials are of growing research interest owing to many applications such as lasers [1, 2], display devices [3], lighting technology [4], solar energy conversion [5], telecommunications [6], remote sensing [7], and laser cooling of solids [8, 9]. In addition to various RE ions, ytterbium (Yb^{3+}) ions are frequently used for high-power infrared fiber lasers, photovoltaic and thermal materials, phosphors, glasses, and unique nanomaterials for medical [10] and biotechnology applications [11]. The Yb^{3+} ion has an absorption band in the near-infrared at 980 nm, enabling the design of materials to be used as spectral converters inefficient solar cells. Glasses doped with Yb^{3+} materials may find technical applications in telecommunications and optical fiber light sources [12].

Yb^{3+}-doped materials are essential in diode-pumped solid-state laser (DPSSL) research. These materials are more suitable for today's new high-energy laser applications than Nd^{3+} materials due to the moderate electronic level structure of Yb^{3+} ions with only two energy states, $^2F_{7/2}$ and $^2F_{5/2}$ [13]. Nd^{3+} and Yb^{3+} materials have minor quantum defects, long lifetimes, and wide bandwidths. Nevertheless, this offer establishes the potential use of Yb^{3+}-doped materials in innovative 'ultrafast' laser generation. However, doping with Yb^{3+} ions presents several problems. Among them a strong influence of the host matrix on spectral and laser properties [14].

In high-power glass-based lasers, phosphate glass is mainly used as the matrix for Yb^{3+} ions due to its high RE ion solubility, gain factor and excellent spectral properties. However, the main drawbacks of phosphate glasses are their chemical robustness and thermos-mechanical limitations.

✉ Ravi Nirlakalla
ravi2728@gmail.com

[1] Department of Physics, Jawaharlal Nehru Technological University, Anantapur 515002, India

[2] Department of Physics, Sreenivasa Institute of Technology and Management Studies, Chitoor 517127, India

[3] Department of Physics, Rajeev Gandhi Memorial College of Engineering and Technology, Nandyal 518501, India

The literature has reported that the mechanical properties of phosphate glasses are effectively improved by doping with SiO_2. Furthermore, the Stark cleavage of Yb^{3+}-doped phosphate glasses was enhanced by including SiO_2 material, allowing the glasses to reach the laser energy effectively. On the other hand, the glass composition and local coordination of RE ions are effectively controlled by SiO_2 doping in phosphate-based glasses, which adversely affects the spectral properties of glasses [15]. Created by Jinhang Wang et al. [16] fabrication process of Er^{3+}/Yb^{3+} phosphor–silicate glass by 3D printing with digital photo processing (DLP) based on sol–gel technology.

Novel glass hosts are indispensable for enhancing Nd laser emission cross-section and bandwidth. In addition, Nd glass fibers based on fluoride are attributed to low signal transmission loss in the NIR region. Mainly, various glasses doped with Nd^{3+} ions exhibit three NIR emission bands at around 0.94, 1.06 and 1.34 µm corresponding to the transmissions from higher energy state $^4F_{3/2}$ to the lower energy states $^4I_{9/2}$, $^4I_{11/2}$, and $^4I_{13/2}$, respectively. However, 1.06 µm band fluorescence is used for high-power laser applications whereas to produce a high-power source by frequency doubling of blue light, in addition, 0.92 µm radiation for pumping ytterbium-doped fiber lasers and amplifiers at 0.98 µm and using Raman fiber lasers as frequency converters [17–19].

In the current work, Yb_2O_3- and Nd_2O_3-doped phospho–silicate (PNSB, PNSBY, $PNSBYNd_{0.5}$, $PNSBYYb_{0.5}$, and $PNSBYNd_{0.5}Yb_{0.5}$) oxyfluoride glasses were synthesized and used SEM, EDS, XPS, and photoluminescence techniques to characterize the morphology, binding energy, valence state, and emission properties.

2 Experimental procedure

Nd/Yb codoped phospho-silicate oxyfluoride glasses made by melt-quench technique. The composition of the glass and the labels are given below. All the chemicals are procured from Alpha Asar with an average assay of 99–99.99%. A total composition mass of 15 g was placed in an agate mortar and then ground for 2 h to obtain a homogeneous powder. Furthermore, this homogeneous powder was placed in an aluminum crucible and then melted at 1200–1300 °C for one hour using an electric furnace. After, the melt was abruptly removed from the furnace and quenched in the air on a brass plate at room temperature (RT). Additionally, these samples were annealed at 350 °C for 10 h and cooled to room temperature to release the stresses of the glasses. These samples were polished for optical quality for photoluminescence and powders for thermal and structural characterizations.

1. $60\ P_2O_5 + 25\ NaF_2 + 10\ SiO_2 + 5\ Bi_2O_3$ (PNSB),
2. $55\ P_2O_5 + 25\ NaF_2 + 10\ SiO_2 + 5\ Bi_2O_3 + 5\ YF_3$ (PNSBY),
3. $54.5\ P_2O_5 + 25\ NaF_2 + 10\ SiO_2 + 5\ Bi_2O_3 + 5\ YF_3 + 0.5\ Yb_2O_3$ ($PNSBYYb_{0.5}$),
4. $54.5\ P_2O_5 + 25\ NaF_2 + 10\ SiO_2 + 5\ Bi_2O_3 + 5\ YF_3 + 0.5\ Nd_2O_3$ ($PNSBYNd_{0.5}$),
5. $54\ P_2O_5 + 25\ NaF_2 + 10\ SiO_2 + 5\ Bi_2O_3 + 5\ YF_3 + 0.5Nd_2O_3/0.5\ Yb_2O_3$ ($PNSBYNd_{0.5}Yb_{0.5}$).

3 Characterization techniques

A scanning electron microscope (JEOL JSM-IT500) with an embedded EDS device was utilized to explore the elemental analysis. The elemental compositions as well as electronic states of the elements of the prepared glasses, including their binding energies were examined by XPS (Model: PHI 5000 Versa Probe II, FEI Inc.) with AES Module (Ar ion as well as C60 sputter guns). Brolight portable optical spectrometer (300–1100 nm) was used to record the photoluminescence of glasses upon 808 and 915 nm laser excitation.

4 Results and discussion

4.1 XRD

X-ray diffraction (XRD) profile of the PNSB glass is displayed in Fig. 1. The profile possesses few humps only; no abrupt peaks that indicates crystallinity were found. This indicates that the glass is highly disordered structure and confirms its non-crystallinity.

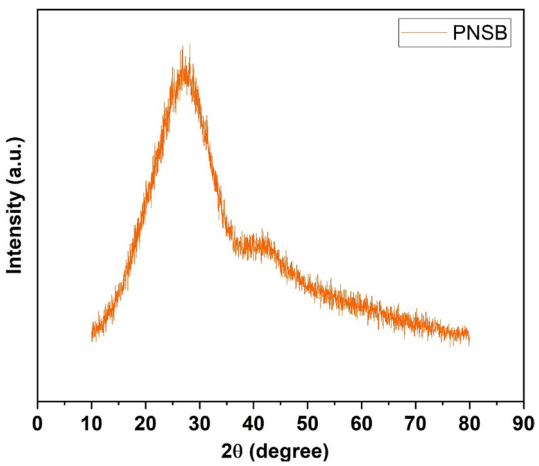

Fig. 1 X-ray diffraction pattern of PNSB glass

4.2 SEM and EDS analyses

The amorphous nature of PNSB glass is shown in Fig. 2a at 20 µm scale. Rigid structure refers to the amorphous nature of the manufactured glass. All elements in the composition of the PNSB glass are shown in the EDS spectrum of Fig. 2b. A strong peak is observed in the EDS spectrum due to the high content of vitrified phosphate. A small amount of aluminum (Al) is seen in the spectrum because the crucible is made of aluminum oxide. Carbon and nitrogen, on the other hand, are produced during sample preparation. The percentage of elemental presence was recorded during the measurement of the EDS spectra. Carbon (C), oxygen (O) and phosphate (P) have high weight percentages (%) presented in the table shown in Fig. 2c.

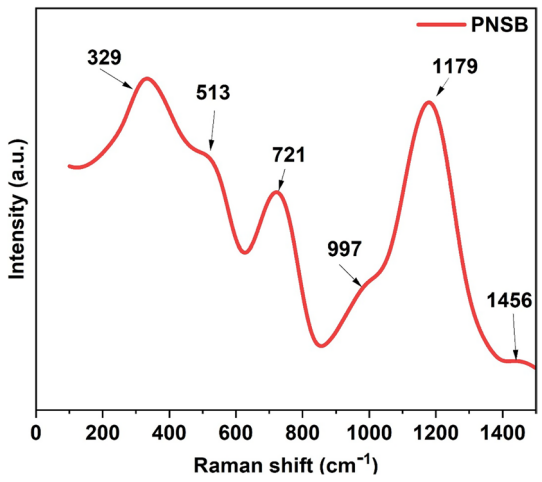

Fig. 3 Raman spectrum of PNSB glass

4.3 Raman spectrum

Raman spectrum of PNSB glass was measured under 514 nm laser excitation in the frequency range of 100–1500 cm^{-1}, as shown in Fig. 3. Raman spectrum of PNSB glass perceived seven bands positioned at 329, 513, 721, 997, 1179, and 1456 cm^{-1}. These bands are well resolved and the Raman band at 339 cm^{-1} is associated with Bi–O bond of BiO_6 octahedra for PNSB glass [20–24]. A small band at 512 cm^{-1} is ascribed to Si–O vibrations [25]. The band at 722 cm^{-1} is due to υ_s(P–O–P) stretching vibration from bridging oxygen (BO) due to Q^1 units for PNSB glass and υ_s(Si–O–Si) stretching vibration from silicon. A band with asymmetrical υ_{as}(P–O–P) stretching of non-bridging oxygen (NBO) was observed at 997 cm^{-1} in PNSB glass. Raman bands positioned at higher-frequency region (> 1000 cm^{-1}) are because of localized Si–O stretching vibrations of tetrahedral silicates [26]. A high-intense and broad band at 1184 cm^{-1} is attributed to υ_{as}(Si–O–Si) stretching vibrations of Q^3 units owing to high-alkali (Na^+) silicates [27] and O–P–O $(PO)^{2-}$ symmetric stretching vibrations in Q^2 units. A weak band was found at 1456 cm^{-1} due to stretching of NBO in Q^3 tetrahedra ν(P=O) (Q^3) [28].

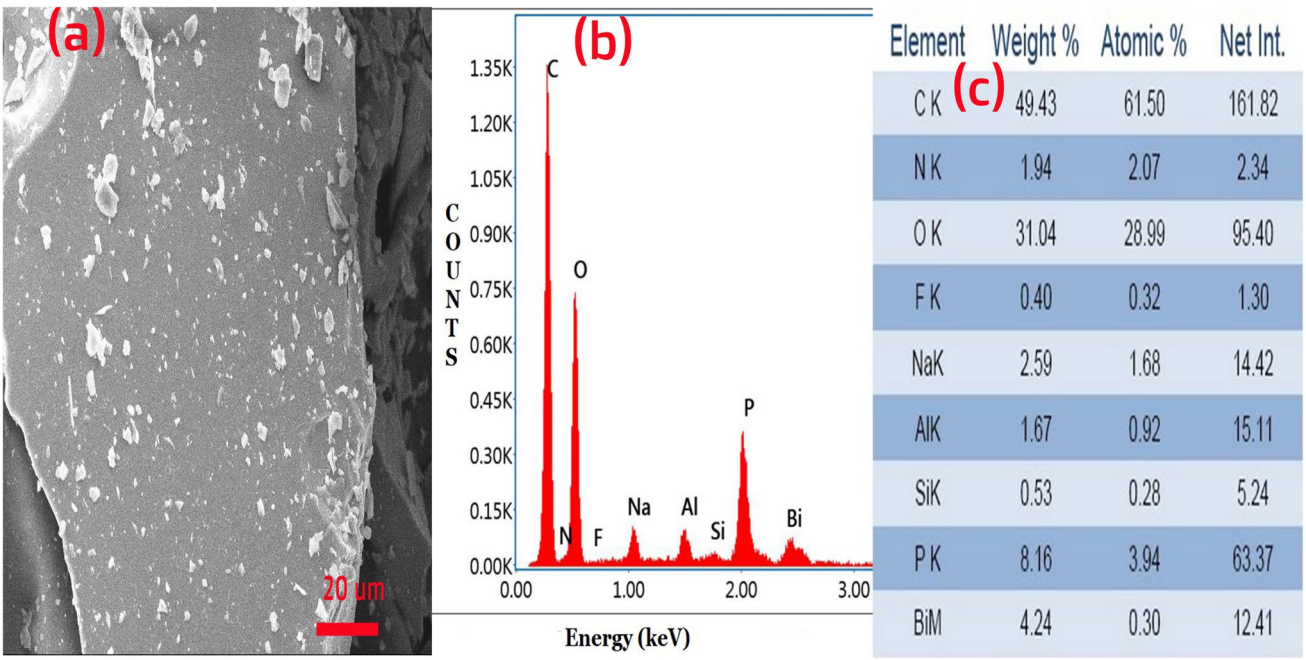

Element	Weight %	Atomic %	Net Int.
C K	49.43	61.50	161.82
N K	1.94	2.07	2.34
O K	31.04	28.99	95.40
F K	0.40	0.32	1.30
NaK	2.59	1.68	14.42
AlK	1.67	0.92	15.11
SiK	0.53	0.28	5.24
P K	8.16	3.94	63.37
BiM	4.24	0.30	12.41

Fig. 2 Morphological structure of Bi^{3+} ions-doped phospho–silicate (PNSB) glass. **a** SEM micrograph, **b** elemental mapping (EDS) spectra and **c** table of elements with their percentage

4.4 ESR spectrum

Electron spin resonance (ESR) spectrum of PNSBY glass was studied for magnetic behavior and free electron availability in the Q-band region at room temperature under applied 0–0.6 T magnetic field. Adding of 5 mol% YF_3 increases the availability of free electrons, which leads to the magnetic moment. $[Kr]4d^1\ 5s^2$ is the electronic configuration of yttrium (Y) with an angular momentum of 2, a magnetic momentum of − 2, and a spin of + 1/2 exhibits magnetic behavior. Since the crystal field splitting for Y^{3+} is typically smaller than that developed by the Zeeman interaction in X-band ESR experiments. Moreover, the ESR spectrum is depicted as a spin Hamiltonian including the interaction between Zeeman and the crystal field given by Eq. (1).

$$H = H_{\mathrm{ZEEMAN}} + H_{\mathrm{exch}} + H_{\mathrm{SS}},$$

$$H = g_0\mu_{\mathrm{B}}BS + JS_1S_2 + D[S_z^2 - (1/3)S(S+1)] + E\left(S_x^2 - S_y^2\right), \quad (1)$$

where B is the magnetic field, μ_{B} is the Bohr magneton, and S_x, S_y, S_z are electron spin operators, H_{exch} is a Hamiltonian of electron exchange interaction with an isotropic electron exchange coupling constant, J, H_{SS} is a Hamiltonian of dipolar electron spin interaction with D and E being the zero-field splitting constants; the value of g-factor of the Y^{3+} is isotropic and equals to g_0 as in a case of free ion [29, 30]. The d orbitals are uncompressed for iron and manganese compared to the f orbitals of RE^{3+} ions. This leads to a more covalent character of metal–ligand interactions in d-element complexes and also influences the correlation of strength, distribution width and zero-field splitting parameters.

The electron Lande splitting factor (g) or g-factor is the ratio of the electron's magnetic moment to the electron's total spin angular momentum. The magnitude of g is contingent on the orientation of the unpaired electron-containing molecules/ions concerning the applied magnetic field. The g values of unpaired electrons in gas atoms/molecules/ions are given as Russell–Saunders bonds (L–S coupling) and is applied in Eq. (2).

$$g = 1 + \frac{J(J+1) + S(S+1) - L(L+1)}{J(J+1)}. \quad (2)$$

For a free electron, $S = 1/2$, $L = 0$ and $J = 1/2$, the value of g come out to be 2.0 using Eq. (2). The actual value of free electron is 2.0023. For most free radicals, the orbital involvement to the magnetic moment is insignificant and the g-value is around equal to the free electron value of 2.0023. The slight deviation (± 0.05) frequently detected for most free radicals is described as a mixture of low excited and ground states. The properties of transition metals (TM) are evaluated mainly by the relative sizes of the crystalline field and spin–orbit coupling. These two interactions have opposite effects on orbital degeneracy [31].

Fast electron exchange interaction was identified due to its signal behavior. A deviation of the ESR line shape from the Lorentzian due to the scattering effect because of the non-diagonal component of the magnetic susceptibility at a large linewidth of 45 mT. Resonant magnetic field (H_r) occurred at 335.16 mT for PNSBY glasses displayed in Fig. 4a. The g value of PNSBY glasses are observed at 2.0168, 2.1595, 2.9748, and 3.7661. These g values for PNSBY glasses revealed that the availability of free electrons responsible for the paramagnetic behavior of Y^{3+} ions is due to its value being more significant than that of 2.0023 exposed in Fig. 4b.

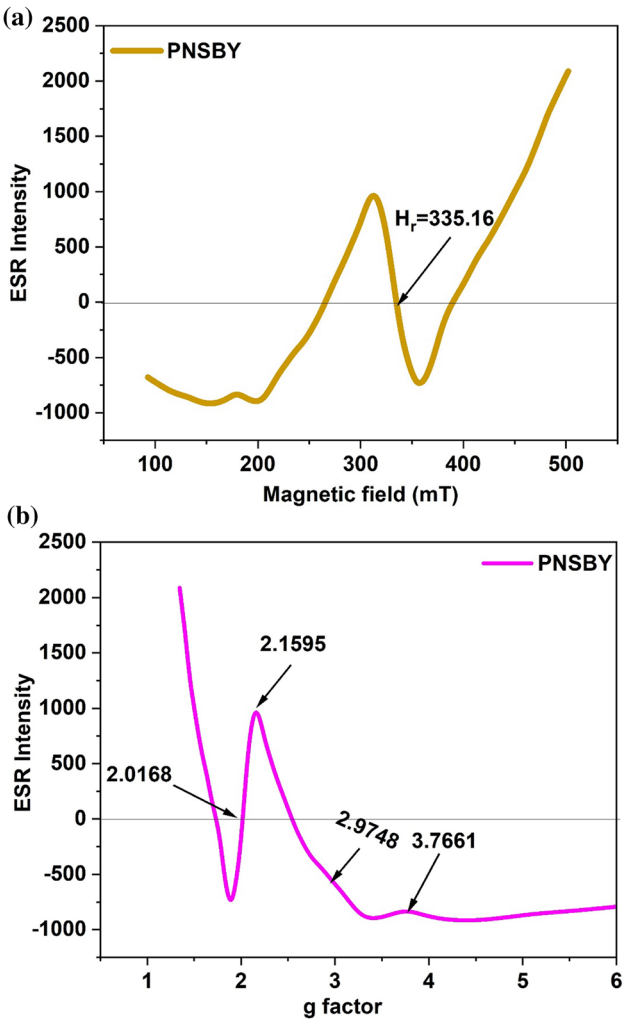

Fig. 4 ESR spectra of **a** magnetic field vs intensity and **b** g-factor vs intensity of 5 mol% Bi_2O_3 and Y_2O_3

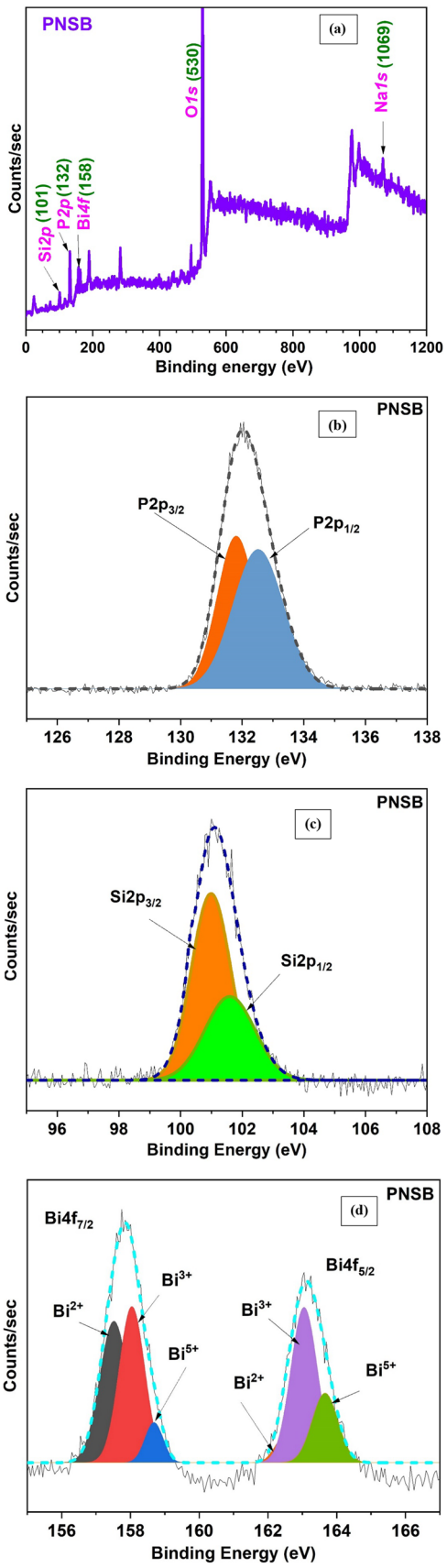

Fig. 5 XPS spectra of **a** PNSB glass and binding energies of **b** P2p, **c** ▸ Si2p and **d** Bi4f

4.5 XPS analysis

Binding energies and valency states of the elements of the PNSB glass were analyzed using X-ray photoelectron spectroscopy (XPS), which revealed binding energy (BE) in the range of 0–1200 eV. Silicon in the Si2*p* state, phosphorous in the P2*p* state, bismuth in the Bi4*f* state, oxygen in the O1*s* state and sodium in the Na1*s* corresponding BEs were revealed at ~ 101 eV, 132 eV, 158 eV, 530 eV, and 1069 eV, respectively for PNSB glass as displayed in Fig. 5a. The PNSB glass exhibits the P2$p_{3/2}$ peak position having BE with phosphate PO_4^{3-} units at 132 eV [32]. Spectral peaks clearly indicate that the glass specifying the prime role of PO_4^{3-} units in the glass is revealed in Fig. 5b with a broad peak. Subsequently, this causes for the existence of P2$p_{3/2}$ to be in a 5 + valance state. Owing to PO_4^{3-} units orthophosphate-type structure in these glasses [33]. The full-width at half-maximum (FWHM) of P2$p_{3/2}$ peak is 1.85 for PNSB glass. When P2*p* of PNSB glass is deconvoluted, it exhibits two peaks positioned at 131.8 and 132.5 eV for 2$p_{3/2}$, and 2$p_{1/2}$, respectively, in which P2$p_{3/2}$ peak was dominated.

Si2p spectra of PNSB glass was shown in Fig. 5c. The BE of the Si2$p_{3/2}$ peak at around 101 eV is due to Q^3 class of bonding units; whereas, the Si2$p_{1/2}$ peak at approximately 101.6 eV is owing to Q^4 class of bonding units. The FWHM of the Si2*p* peak is 2.05 eV for PNSB glass. The BE peaks of Bi for 4$f_{7/2}$ and 4$f_{5/2}$ are centered at 157.75 eV and 163.11 eV, respectively, for PNSB exposed in Fig. 5d. In addition, FWHM of Bi 4$f_{7/2}$ and Bi 4$f_{5/2}$ peaks of PNSB glass are 1.20 and 1.31 eV, respectively. Additionally, when Bi4f peaks were deconvoluted for PNSB glass, the ionic states of Bi ions were found to be Bi^{2+} at 157.5 eV, Bi^{3+} at 158 eV and Bi^{5+} at 158.6 eV for Bi4$f_{7/2}$ and Bi^{2+} at 162 eV, Bi^{3+} at 163 eV and Bi^{5+} at 163.6 eV. However, 3 + ionic states of Bi were dominated and revealed in Bi 4$f_{7/2}$ and Bi 4$f_{5/2}$ peaks of PNSB glass.

4.6 Optical absorption

The optical absorption bands 349, 445, 523, 583, 629, 683, 629, 683, 746, 799, 874, and 973 nm were revealed in neodymium oxide (Nd_2O_3) and ytterbium oxide (Yb_2O_3) Nd/Yb-doped PNSBY$Nd_{0.5}Yb_{0.5}$ in the UV–visible–NIR absorption spectrum measured in the range 270–1100 nm corresponding to the transmissions $^4I_{9/2} \rightarrow {}^2I_{11/2}$, $^2K_{15/2} + {}^4G_{11/2} + {}^2D_{3/2}$, $^4G_{9/2} + {}^4G_{7/2}$, $^2G_{7/2} + {}^4G_{5/2}$, $^2H_{9/2}$, $^4F_{9/2}$, $^4S_{3/2} + {}^4F_{7/2}$, $^4F_{5/2} + {}^2H_{9/2}$, and $^4F_{3/2}$ for Nd^{3+} ions and $^2F_{7/2} \rightarrow {}^2F_{5/2}$ for Yb^{3+} ions displayed in Fig. 6. A broad absorption band was found at 445 nm overlapping of three bands due to $^2K_{15/2} + {}^4G_{11/2} + {}^2D_{3/2}$, three intense peaks were observed at

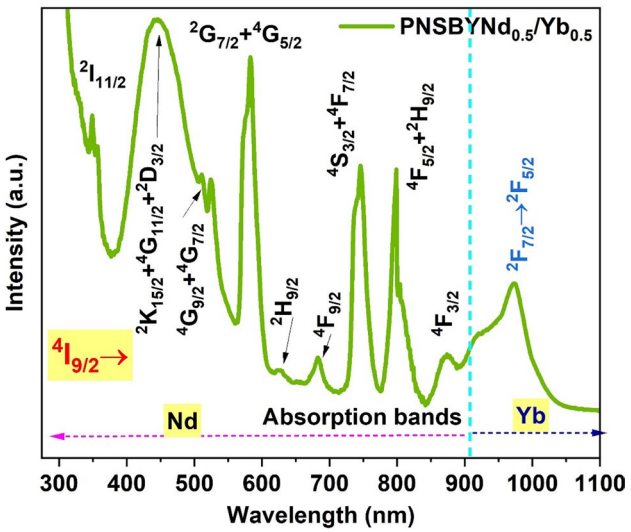

Fig. 6 Optical absosption spectrum of $PNSBYNd_{0.5}Yb_{0.5}$ glass in the range UV–visible–NIR

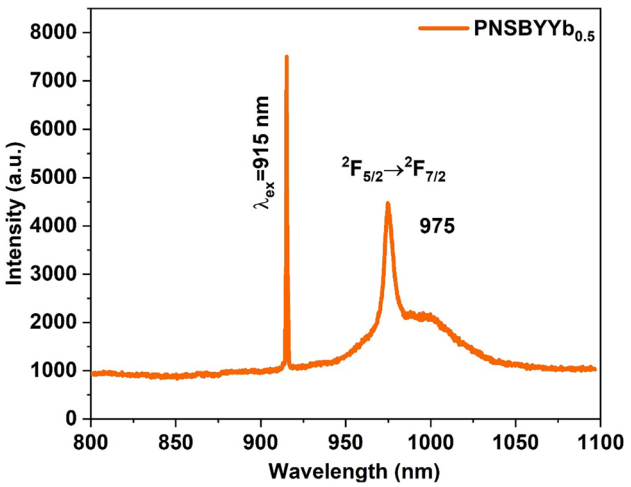

Fig. 7 Emission spectrum of $PNSBYYb_{0.5}$ glass under 915 nm laser excitation

583 ($^2G_{7/2}+{}^4G_{5/2}$), 746 ($^4S_{3/2}+{}^4F_{7/2}$), and 799 ($^4F_{5/2}+{}^2H_{9/2}$) nm. The highest intensity of 583 nm is due to the hypersensitive behavior of Nd^{3+} ions that follows the selection rules of $|\Delta L|\leq 2$, $|\Delta S|\leq 0$ and $|\Delta J|\leq 2$ [17].

4.7 Photoluminescence

The luminescence properties of 0.5 mol% (Nd_2O_3 and Yb_2O_3) embedded in PNSBY glasses were studied. As illustrated in Fig. 7, when Yb^{3+} ions were pumped with a wavelength of approx. 915 nm in the $PNSBYYb_{0.5}$ glass, a broad and intense emission band was observed at 975 nm due to the transitions $^2F_{5/2}\rightarrow{}^2F_{7/2}$. The FWHM of the broad emission band at 975 nm for $PNSBYYb_{0.5}$ glass is about 10.55 nm. The luminescence conversion process obviously depends on the energy transfer (ET) of the RE ions concerning their structure and the local environment. When the RE ion concentration was changed, the fluorescence characteristics caused by ET changed significantly. However, there are few reports on the consequences of structural deformation on the emission mechanism of Y_2O_3:Bi conversion with changes in Yb^{3+} ion concentration [34].

In addition to the broad emission in the NIR region at the active Bi^{3+} binding site, a band at 950–1100 nm was also observed in the $PNSBYYb_{05}$ glass. A simple schematic diagram of the energy level of the Yb^{3+} ion and the occurrence of Yb^{3+} emission, as reported in previous reports, shows an ET process at the NIR Bi^{3+} emission center for the Yb^{3+} ion. In particular, when increasing the amount of Yb_2O_3, the emission intensity of Yb^{3+} ions is similar to that of Bi^{3+} ions, which means that the efficiency of ET is very high [35].

The ionic radii of Y^{3+} ions are around 90 pm, which is very convenient for replacing lanthanides, while the radii of Bi^{3+} and Bi^{5+} ions are 103 and 76 pm, respectively. Adding 5 mol% YF_3 increased the emission intensity of Yb^{3+} compared to increasing the Bi_2O_3 content by 5 mol% in the PNSB glass. This demonstrates that the positions of the Y^{3+} atoms agree well with the Bi^{3+}/Yb^{3+} ions. The high transparency of Y^{3+} ions reduces the absorption of $PNSBYYb_{05}$ glasses, ameliorating the thermal stability, optical properties and structural rigidity of glasses [36–39]. This is may be because of the ET between Y^{3+}, Bi^{3+}, and Yb^{3+} ions. NaF, YF_3, and $NaYF_4$ nanocrystals are expected to form in $PNSBYYb_{05}$ glass prepared in this way [40].

0.5 mol% of Nd_2O_3-doped $PNSBYNd_{05}$ glasses were recorded for PL emission in the range of 750–1100 nm excited by the wavelength of 808 nm diode laser. Two emission bands were observed within the region at 876 nm for the $^4F_{3/2}\rightarrow{}^4I_{9/2}$ transition and 1053 nm for the $^4F_{3/2}\rightarrow{}^4I_{11/2}$ transition displayed in Fig. 8. Highest emission was perceived for $^4F_{3/2}\rightarrow{}^4I_{9/2}$ transition at 876 nm which is near to 0.9 μm that can be very useful for fiber laser in under water communication. Nevertheless, it's not easy to get emission for $^4F_{3/2}\rightarrow{}^4I_{9/2}$ (0.9 μm) transition instead of the usual $^4F_{3/2}\rightarrow{}^4I_{11/2}$ (1.06 μm) transition. This is achieved if the laser functions in a quasi-three-level system and the gain medium in the four-level system for the $^4F_{3/2}\rightarrow{}^4I_{11/2}$ transition will be at all times larger than that of the $^4F_{3/2}\rightarrow{}^4I_{9/2}$ transition [41–45]. In a three-level system, the lower laser level matches with the ground state, in which the unexcited medium absorbs emitted photons. On the other hand, the upper pump level overlaps with the upper laser level in which the absorption at pumping photons saturates [46].

Lasers with lower NIR wavelengths are used for the second-harmonic conversion procedure in the blue spectrum laser emission. This results in the wavelength 800–950 nm

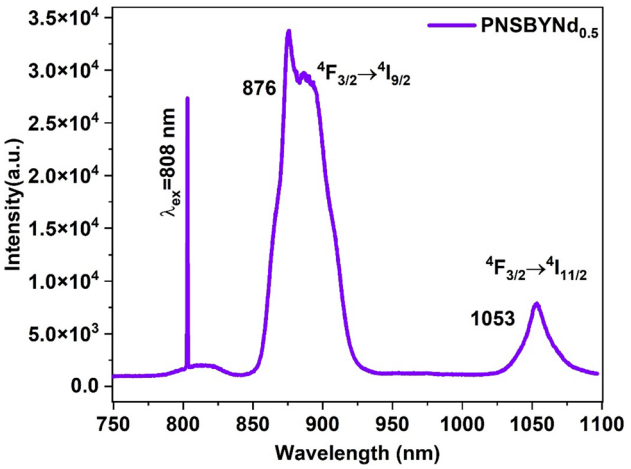

Fig. 8 Emission spectrum of $PNSBYNd_{0.5}$ glass under 808 nm laser excitation

covert into the blue spectrum of 400–445 nm wavelength. Related to diode lasers, this laser shows smaller spectral width and better coherence length, which attracts in the field of interferometer experiments and the sources for the differential absorption lidar (DIAL) in water vapor detection, which has wavelengths overlap the absorption peaks of water vapor [47]. Compared to 1053 nm emission, 876 nm is dominated in the 0.5 mol% Nd_2O_3-doped $PNSBYNd_{05}$ glasses. The Stark effect is the reason for splitting the $^4F_{3/2} \rightarrow {}^4I_{9/2}$ band in the Nd^{3+} ions.

0.5 mol% of each $PNSBYNd_{0.5}Yb_{0.5}$ phospho-silicate oxyfluoride glass doped with Nd_2O_3 and Yb_2O_3 excited in the range 750–1100 nm by 808 nm diode laser is shown in Fig. 9. When Nd^{3+} ions were pumped to a wavelength of 808 nm, they were excited to the $^4I_{9/2} \rightarrow {}^4F_{3/2}$ levels, so the ions were pumped to their closest energy state $^4F_{9/2}$. Furthermore, Nd^{3+} ions were pumped from $^4F_{9/2}$ to $^4I_{11/2}$ by an excited state adsorption (ESA) process illustrated in partial energy level diagram in Fig. 10. Due to the short lifetime of Nd^{3+} ions at the $^2I_{11/2}$ level, they were de-excited in the $^4G_{9/2}$ level via a non-radiative (NR) transition and then de-excited at the $^4F_{3/2}$ level, as shown in Fig. 9. Additionally, the $^4F_{3/2}$ transition with a lifetime longer than the $^4I_{11/2}$ level for Nd^{3+} ions, leading to spontaneous and induced emissions. ET was predicted between the $^4F_{3/2}$ level and the $^2F_{5/2}$ level from Nd^{3+} ions to Yb^{3+} ions due to cross relaxation (CR) and led to emission at the wavelength of 874 nm, which is used for excitation of Yb^{3+} ions.

Three emission bands are detected for $PNSBYNd_{0.5}Yb_{0.5}$ glasses at 874, 975 and 1052 nm corresponding to transitions $^4F_{3/2} \rightarrow {}^4I_{9/2}$, $^2F_{5/2} \rightarrow {}^2F_{7/2}$ and $^4F_{3/2} \rightarrow {}^4I_{11/2}$. Among them, the strong bands at 874 and 1052 nm are due to Nd^{3+} ions, and the highest band at 975 nm is due to Yb^{3+} ions. However, similar emission trends of $PNSBYNd_{05}$ glasses were reported for $PNSBYNd_{0.5}Yb_{0.5}$ glasses. A slight band shift and decreased band intensity at 1053 nm were observed toward the lower wavelength range (1052 nm). This suggests that ET takes place from the Nd^{3+} ions $^4F_{3/2} \rightarrow {}^4I_{11/2}$ transitions to Yb^{3+} ions $^2F_{5/2} \rightarrow {}^2F_{7/2}$; apart from this, ET also observed between the transitions from Nd^{3+} ions $^4F_{3/2} \rightarrow {}^4I_{9/2}$ transitions to Yb^{3+} ions $^2F_{5/2} \rightarrow {}^2F_{7/2}$ transitions displayed in Fig. 10. As a result, the intensity of the Yb band at 975 nm increases and shows greater intensity than the others.

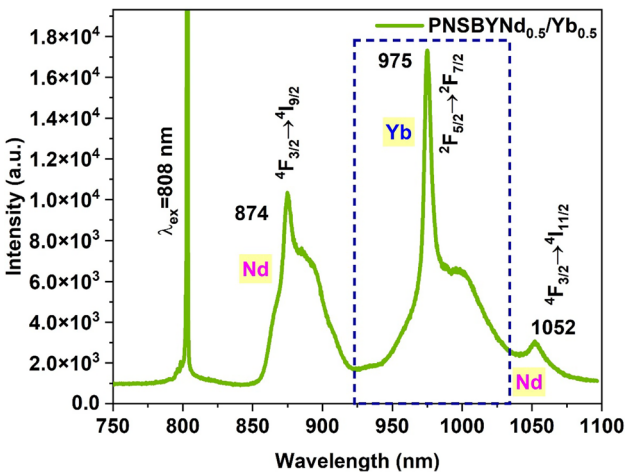

Fig. 9 Emission spectrum of $PNSBYNd_{0.5}Yb_{0.5}$ glass under 915 nm laser excitation

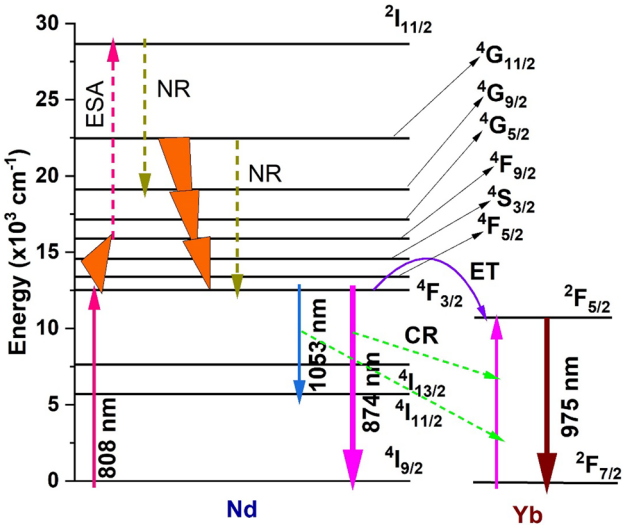

Fig. 10 Partial energy level diagram of Nd and Yb ions in $PNSBYNd_{0.5}Yb_{0.5}$ under 808 nm laser excitation

5 Conclusion

Phospho-silicate oxyfluoride glasses (PNSBY) doped with Nd/Yb ions were explored for elemental analysis, phosphate and bismuth ion binding energies, and photoluminescence properties. The solid, stone-like morphology confirmed the amorphous behavior of the PNSB glass. EDS spectrum was used to monitor the elemental compositions and their concentrations. A $P2p_{3/2}$ valence state is observed in the phosphorus XPS spectrum. In the XPS spectrum, the content of Bi, F and more oxygen were the reason for changes in the binding energy values from the actual values of the PNSB glass. Two spectral peaks of Bi $^4F_{5/2}$ and $^4F_{7/2}$ were visible in this glass. In a 0.5 mol% Yb_2O_3-doped $PNSBYYb_{0.5}$ glass, a broad emission band at 975 nm was observed when Yb^{3+} ions were excited by the wavelength of 915 nm diode laser. A 0.5 mol% of Nd_2O_3-doped $PNSBYNd_{0.5}$ glass emits at 876 nm owing to $^4F_{3/2} \rightarrow {}^4I_{9/2}$ band was dominated compared to 1053 nm band due to quasi-three-state system of Nd^{3+} ions in $PNSBYNd_{0.5}$ glasses. Nd/Yb-codoped $PNSBYNd_{0.5}Yb_{0.5}$ glasses were investigated for energy transfer studies, those have shown ET from $^4F_{3/2}$ to $^4F_{7/2}$, and the intensity of Yb band at 975 nm was enhanced due to CR from 1053 and 876 nm. As a result, the emission at 975 nm is beneficial for developing 1.0 μm laser and amplifiers for under water communication applications.

Data availability Data is available at the corresponding author and will be provided only on request basis.

References

1. V. Thomas, R.G.S. Sofin, M. Allen, H. Thomas, P.R. Biju, G. Jose, N.V. Unnikrishnan, Optical analysis of samarium doped sodium bismuth silicate glass. Spectrochim. Acta Mol. Biomol. Spectrosc. **171**, 144–148 (2017)
2. I. Iparraguirre, J. Azkargorta, R. Balda, K. Venkata Krishnaiah, C.K. Jayasankar, M. Al-Saleh, J. Fernández, Spontaneous and stimulated emission spectroscopy of a Nd^{3+}-doped phosphate glass under wavelength selective pumping. Opt. Express **19**, 19441 (2011)
3. C.R. Kesavulu, H.J. Kim, S.W. Lee, J. Kaewkhao, N. Chanthima, Y. Tariwong, Physical, vibrational, optical and luminescence investigations of Dy^{3+}-doped yttrium calcium silicoborate glasses for cool white LED applications. J. Alloy. Compd. **726**, 1062–1071 (2017)
4. B. Peng, L. Jiang, X.M. Qiu, Z.C. Fan, W. Huang, Ytterbium doped heavy metal oxide glasses with high emission cross-section. J. Alloy. Compd. **398**, 170–172 (2005)
5. K. Venkata Krishnaiah, P. Venkatalakshmamma, Ch. Basavapoornima, I.R. Martín, K. Soler-Carracedo, M.A. Hernández-Rodríguez, V. Venkatramu, C.K. Jayasankar, Er^{3+}-doped tellurite glasses for enhancing a solar cell photocurrent through photon upconversion upon 1500 nm excitation. Mater. Chem. Phys. **199**, 67–72 (2017)
6. S. Yoo, M.P. Kalita, A.J. Boyland, A.S. Webb, R.J. Standish, J.K. Sahu, M.C. Paul, S. Das, S.K. Bhadra, M. Pal, Ytterbium-doped Y_2O_3 nanoparticle silica optical fibers for high power fiber lasers with suppressed photodarkening. Opt. Commun. Commun. **283**(18), 3423–3427 (2010)
7. B. Klimesz, R. Lisiecki, W. Ryba-Romanowski, Thermal, spectroscopic and optical sensor properties of oxyfluorotellurite glasses doped with holmium and ytterbium. Mater. Res. Bull. **153**, 111909 (2022)
8. E.S. de Lima Filho, K.V. Krishnaiah, Y. Ledemi, Y.-J. Yu, Y. Messaddeq, G. Nemova, R. Kashyap, Ytterbium-doped glass-ceramics for optical refrigeration. Opt. Express **23**, 4630 (2015)
9. K.V. Krishnaiah, E.S. de LimaFilho, Y. Ledemi, G. Nemova, Y. Messaddeq, R. Kashyap, Development of ytterbium-doped oxyfluoride glasses for laser cooling applications. Sci. Rep. **6**, 21905 (2016)
10. P. Kowalik, I. Kamińska, K. Fronc, A. Borodziuk, M. Duda, T. Wojciechowski, K. Sobczak, D. Kalinowska, M.T. Klepka, B. Sikora, The ROS-generating photosensitizer-free NaYF4:Yb, $Tm@SiO_2$ upconverting nanoparticles for photodynamic therapy application. Nanotechnology **32**, 475101 (2021)
11. Y.C. Dong, A. Kumar, D.N. Rosario-Berríos, S. Si-Mohamed, J.C. Hsu, L.M. Nieves, P. Douek, P.B. Noël, D.P. Cormode, Ytterbium nanoparticle contrast agents for conventional and spectral photon-counting CT and their applications for hydrogel imaging. ACS Appl. Mater. Interfaces **14**, 34 (2022)
12. I.D. Zakiryanova, D.O. Zakiryanov, Ab initio molecular dynamics simulations and Raman spectra of the $YbCl_3$–KCl and Yb_2O_3–$YbCl_3$–KCl ionic melts. J. Mol. Liq. **318**, 114054 (2020)
13. K. Venkata Krishnaiah, C.K. Jayasankar, S. Chaurasia, C.G. Murali, L.J. Dhareshwar, Preparation and characterization of Yb^{3+}-doped metaphosphate glasses for high energy and high power laser applications. Sci. Adv. Mater. **5**, 276–284 (2013)
14. A. Prnováa, K. Bodišová, R. Klement, M. Migát, P. Veteškab, M. Škrátek, E. Bruneel, I. VanDriessche, D. Galusek, Preparation and characterization ofYb_2O_3–Al_2O_3 glasses by the Pechini sol–gel method combined with flame synthesis. Ceram. Int. **40**, 6179–6184 (2014)
15. L. Wang, H. Zeng, B. Yang, F. Ye, J. Chen, G. Chen, A.T. Smith, L. Sun, Structure-dependent spectroscopic properties of Yb^{3+}–doped phosphosilicate glasses modified by SiO_2. Materials **10**, 241 (2017)
16. J. Wang, B. Zheng, P. Wang, 3D printed Er^{3+}/Yb^{3+} co-doped phosphosilicate glass based on sol-gel technology. J. Non-Cryst. SolidsCryst. Solids **550**, 120362 (2020)
17. G. Neelima, K. Venkata Krishnaiah, N. Ravi, K. Suresh, K. Tyagarajan, T. Jayachandra Prasad, Investigation of optical and spectroscopic properties of neodymium doped oxyfluoro-titania-phosphate glasses for laser applications. Scr. Mater. **162**, 246–250 (2019)
18. Z.A.S. Mahraz, E.S. Sazali, M.R. Sahar, N.U. Amran, S.N.S. Yaacob, S.M. Aziz, S.Q. Mawlud, F.M. Noor, A.N. Harun, Spectroscopic investigations of near-infrared emission from Nd^{3+}-doped zinc-phosphate glasses: Judd–Ofelt evaluation. J. Non-Cryst. SolidsCryst. Solids **509**, 106–114 (2019)
19. D.B.S. Soh, S. Yoo, J. Nilsson, J.K. Sahu, K. Oh, S. Baek, Y. Jeong, C. Codemard, P. Dupriez, J. Kim, V. Philippov, Neodymium-doped cladding-pumped aluminosilicate fiber laser tunable in the 0.9-μm wavelength range. IEEE J. Quantum Electron. **40**(9), 1275–1282 (2004)
20. L. Baia, R. Stefan, W. Kiefer, S. Simon, Structural characteristics of B_2O_3–Bi_2O_3 glasses with high transition metal oxide content. J. Raman Spectrosc.Spectrosc. **36**, 262–266 (2005)
21. D. Manzani, C.B. de Araujo, G. Boudebs, Y. Messaddeq, S.J.L. Ribeiro, The role of Bi_2O_3 on the thermal, structural, and optical

properties of tungsten-phosphate glasses. J. Phys. Chem. B **117**, 408–414 (2013)
22. A. Mandlule, F. Döhler, L. van Wüllen, T. Kasuga, D.S. Brauer, Changes in structure and thermal properties with phosphate content of ternary calcium sodium phosphate glasses. J. Non-Cryst. SolidsCryst. Solids **392–393**, 31–38 (2014)
23. H. El Hamzaoui, C. Kinowski, I. Razdobreev, A. Cassez, G. Bouwmans, B. Prochet, B. Capoen, M. Bouazaoui, Synthesis, structural and optical properties of bismuth-doped sol–gel-derived phosphosilicate glasses. Phys. Status Solidi A **216**, 1800411 (2018)
24. S. Chakraborty, A.K. Arora, Temperature evolution of Raman spectrum of iron phosphate glass. Vib. Spectrosc.Spectrosc. **61**, 99–104 (2012)
25. T. Seuthe, M. Grehn, A. Mermillod-Blondin, H.J. Eichler, J. Bonse, M. Eberstein, Structural modifications of binary lithium silicate glasses upon femtosecond laser pulse irradiation probed by micro-Raman spectroscopy. Opt. Mater. Express **73**(6), 755–764 (2013)
26. C.M. Calahoo, J.W. Zwanziger, I.S. Butler, Mechanical-structural investigation of ion-exchanged lithium silicate glass using micro-raman spectroscopy. J. Phys. Chem. C **120**(13), 7213–7232 (2016)
27. D.W. Matson, S.K. Sharma, J.A. Philpotts, The structure of high-silica alkalisilicate glasses. A Raman spectroscopic investigation. J. Non-Cryst. SolidsCryst. Solids **58**(2–3), 323–352 (1983)
28. Y. Yue, Y. Wang, Y. Cao, S. Chen, Q. Zhou, W. Chen, L. Hu, Effect of Al_2O_3 on structure and properties of Al_2O_3–K_2O–P_2O_5 glasses. Opt. Mater. Express **8**(2), 245–258 (2018)
29. J.A. Weil, J.R. Bolton, *Electron Paramagnetic Resonance. Elementary Theory and Practical Applications*, 2nd edn. (Wiley, Hoboken, 2007), p.158
30. G. Leniec, L. Macalik, S.M. Kaczmarek, T. Skibinski, J. Hanuza, EPR and optical properties of $KY(WO_4)_2$:Gd^{3+} powders. J. Mater. Res. **27**(23), 2973–2981 (2012)
31. C.N. Banwell, E.M. Mc Cash, *Fundamentals of Molecular Spectroscopy*, 4th edn. (Tata McGraw-Hill Publishing, New Delhi, 1996)
32. G.D. Khattak, M.A. Salim, A.S. Al-Harthi, D.J. Thompson, L.E. Wenger, Structure of molybdenum-phosphate glasses by X-ray photoelectron spectroscopy (XPS). J. Non-Cryst. SolidsCryst. Solids **212**, 180–191 (1997)
33. http://www.xpsfitting.com/2013/01/phosphorus.html
34. Z. Yongminga, L. Yanhonga, Z. Yanga, H. Guangyanb, Y. Yingning, Effect of Yb^{3+} concentration on the structures and upconversion luminescence properties of Y_2O_3:Er^{3+} ultrafine phosphors. Rare Met. **27**(6), 603 (2008)
35. C. Li, J. Qiu, Z. Song, Qi. Wang, X. Wang, Y. Li, Z. Yang, Z. Yin, D. Zhou, Effects of Yb_2O_3 on the NIR emission performance of Bi–Yb codoped aluminophosphosilicate glasses. J. Non-Cryst. SolidsCryst. Solids **383**, 169–172 (2014)
36. A. Arafat, S.A. Samad, M.D. Wadge, M.T. Islam, A.L. Lewis, E.R. Barney, I. Ahmed, Thermal and crystallization kinetics of yttrium-doped phosphatebased Glasses. Int J. Appl. Glass Sci. **11**(1), 120–133 (2020)
37. Z. Zou, Wu. Ting, Lu. Hao, Tu. Yuyuan, S. Zhao, S. Xie, F. Han, Xu. Shiqing, Structure, luminescence and temperature sensing in rare earth doped glass ceramics containing $NaY(WO_4)_2$ nanocrystals. RSC Adv. **8**, 7679–7686 (2018)
38. Y. Cheng, C. Yu, H. Dong, S. Wang, C. Shao, Y. Sun, S. Sun, Y. Shen, J. Cheng, L. Hu, Spectral properties of ultra-low thermal expansion Er^{3+}/Yb^{3+} co-doped phosphate glasses. Ceram. Int. **49**(11(B)), 18305–18310 (2023)
39. J.A. Jiménez, Physical and spectroscopic properties of variable Yb_2O_3 doped phosphate glasses containing SnO as UV sensitizer for Yb^{3+} NIR emission. Opt. Mater. **141**, 113984 (2023)
40. C.N. Santos, D. De Sousa, P.E. Meneses, D.R. Neuville, A.C. Hernandes, A. Ibanez, Structural, dielectric, and optical properties of yttrium calcium borate glasses. Appl. Phys. Lett. **94**, 151901 (2009)
41. I.A. Bufetov, V.V. Dudin, A.V. Shubin, A.K. Senatorov, E.M. Dianov, A.B. Grudinin, S.E. Goncharov, I.D. Zalevskii, A.N. Gur'yanov, M.V. Yashkov, A.A. Umnikov, N.N. Vechkanov, Efécient 0.9-lm neodymium-doped single-mode ébre laser. Quantum Electron. **33**(12), 1035–1037 (2003)
42. S. Han, X. Li, H. Xu, Y. Zhao, H. Yu, H. Zhang, Y. Wu, Z. Wang, X. Hao, X. Xu, Graphene Q-switched 0.9-μm Nd:$La_{0.11}Y_{0.89}VO_4$ laser. Chin. Opt. Lett. **12**(1), 011401 (2014)
43. N. Pavel, K. Lünstedt, K. Petermann, G. Huber, Multipass pumped Nd-based thin-disk lasers: continuous-wave laser operation at 1.06 and 0.9 μm with intracavity frequency doubling. Appl. Opt. **46**(34), 8256–8263 (2007)
44. M.M. Ismail, Y.M. Hamdy, H.A. Abo-Mosallam, Enhancing of $^4F_{3/2} \rightarrow {}^4I_{9/2}$ transition of Nd^{3+} doped BaO–Ga_2O_3–Al_2O_3–B_2O_3 glasses for near-infrared laser applications. J. Lumin. **263**, 120014 (2023)
45. Y. Yue, M. Fu, Y. Yang, W. Chen, L. Hu, M. Guzik, G. Boulon, Effect of silica-alumina co-introduction on structure as well as physical and spectroscopic properties of Nd^{3+}-doped potassium phosphate glass. J. Non-Cryst. SolidsCryst. Solids **610**, 122306 (2023)
46. J.O. White, Parameters for quantitative comparison of two-, three-, and four-level laser media, operating wavelengths, and temperatures. IEEE J. Quantum Electron. **45**(10), 1213–1220 (2009)
47. Y. Tan, F. Chen, J.R. Vázquez, H. de Aldana, Yu and Huaijin-Zhang, Quasi-three-level laser emissions of neodymium doped disordered crystal waveguides. IEEE J. Sel. Top. Quantum Electron. **21**(1), 1601905 (2015)